Atmospheric Pollution Research 16 (2025) 102330

Contents lists available at ScienceDirect

Atmospheric Pollution Research

journal homepage: www.elsevier.com/locate/apr

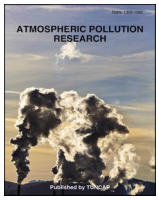

Size-segregated particulate matter oxidative potential near a ferromanganese plant: Associations with soluble and insoluble elements and their sources

A. Expósito [a], E. Vaccarella [b], L. Massimi [b,c], M. Santibáñez [d,e], I. Fernández-Olmo [a,*]

[a] Department of Chemical and Biomolecular Engineering, Universidad de Cantabria, Santander, 39005, Spain
[b] Department of Environmental Biology, Sapienza University of Rome, P. le Aldo Moro, 5, Rome, 00185, Italy
[c] C.N.R. Institute of Atmospheric Pollution Research (CNR-IIA), Via Salaria, Km 29, 300, Monterotondo St., Rome, 00015, Italy
[d] Global Health Research Group, Department of Nursing, Universidad de Cantabria, Santander, 39008, Spain
[e] Nursing Research Group, IDIVAL, Calle Cardenal Herrera Oria s/n, 39011, Santander, Cantabria, Spain

ARTICLE INFO

Keywords:
Particulate matter
Oxidative potential
Ascorbic acid
Dithiothreitol
2,7-Dichlorofluorescein

ABSTRACT

The oxidative potential (OP) of particulate matter (PM) is considered a better health metric of PM exposure than mass concentration since its value is highly dependent on PM composition. OP assays have shown different sensitivities to PM components and particle sizes. In this work, an urban-industrial mixed site with high levels of airborne Mn and Fe, due to the proximity of a ferromanganese alloy plant, was chosen to study the association between PM elements and three OP assays (ascorbic acid (AA), dithiothreitol (DTT), and 2,7-dichlorofluorescein (DCFH)) in size segregated PM samples ($PM_{10\text{-}2.5}$ and $PM_{2.5}$). Urban samples from a nearby area were also collected. The concentration of 39 elements in both the soluble (in a phosphate buffer aqueous solution) and insoluble fractions of $PM_{10\text{-}2.5}$ and $PM_{2.5}$ was determined by ICP-MS. Soluble elements were then associated with OP and local sources using Principal Component Analysis (PCA). Four sources of soluble elements have been identified in the urban-industrial site. The main factor was attributed to road traffic; although Cu and Fe, two active transition metals in OP assays, were associated to this factor, their low solubility, mainly in the coarse fraction, has led to low factor loadings of OP; the second factor was attributed to a ferromanganese plant, since it presented the highest factor loadings for soluble Mn in both $PM_{10\text{-}2.5}$ and $PM_{2.5}$; it was the main factor associated with OP-DTT and OP-DCFH values, mainly in the coarse fraction. Crustal material and sea salt aerosol were also identified as sources.

1. Introduction

Particulate matter (PM), and mainly its fine fraction ($PM_{2.5}$) are considered the major contributors to morbidity and mortality among the regulated air pollutants (Dockery and Pope, 1994; Lelieveld et al., 2015; Ostro et al., 2006; WHO, 2021). Particle size and chemical composition of PM are responsible for the toxic effects linked to PM exposure (Kelly and Fussell, 2012; Li et al., 2019); however, the toxicity mechanisms are not fully understood (Feng et al., 2016). In addition, the current regulation (at least in the European Union) only sets limit/target values for PM mass concentration (PM_{10} and $PM_{2.5}$) and for some PM-bound minor pollutants, such as As, Cd, Ni, Pb, and benzo(a)pyrene (Directives 2004/107/EC and 2008/50/EC). For these reasons, the use of a toxicity-based metric for PM has gained interest in the last decade, not only for research interests but also for regulation purposes. Thus, the measurement of the PM oxidative potential (OP) in supersites has been suggested in the revision of Directive 2008/50/EC - Proposal for a Directive of the European Parliament and of the Council on ambient air quality and cleaner air for Europe - (European Parliament, 2022), because it will support scientific understanding of the effects of PM exposure on health. The so-called OP is defined as the ability of inhaled PM components to produce reactive oxygen species (ROS) while simultaneously depleting cellular antioxidants (Bates et al., 2019).

In the last years, PM OP has been considered a better health-based metric of PM exposure than PM mass concentration (Bates et al., 2019; Daellenbach et al., 2020; Molina et al., 2020). Cell-based

Peer review under responsibility of Turkish National Committee for Air Pollution Research and Control.
* Corresponding author.
E-mail address: fernandi@unican.es (I. Fernández-Olmo).

https://doi.org/10.1016/j.apr.2024.102330
Received 12 April 2024; Received in revised form 8 October 2024; Accepted 8 October 2024
Available online 16 October 2024

(cellular) and cell-free (acellular) assays have been developed in the last decades to determine the OP of PM. Acellular assays have been more widely applied in the literature due to their simplicity, fastness, and lower cost compared to cellular assays (Bates et al., 2019; Pietrogrande et al., 2019). The most commonly used acellular assay is based on the consumption of dithiothreitol (DTT), a surrogate of cellular reductant that contains thiol groups (Cho et al., 2005; Jiang et al., 2019). Other assays are based on the depletion of natural antioxidants present in lung fluids, such as ascorbic acid (AA) and reduced glutathione (GSH) (Bates et al., 2019; Pietrogrande et al., 2019; Szigeti et al., 2015), or on the determination of ROS, such as hydrogen peroxide (H_2O_2); among the later ones, the 2,7-dichlorofluorescein (DCFH) assay has been widely applied to PM samples (Crobeddu et al., 2017; Frezzini et al., 2022; Jovanovic et al., 2019; Khurshid et al., 2014; Perrone et al., 2016). Despite the widespread use of various OP assays, they showed important differences in their sensitivities to the studied samples, and therefore OP results from various assays may be considered complementary (Simonetti et al., 2018; Shahpoury et al., 2022).

These differences are mainly attributed to the changes in the chemical composition of PM because it strongly affects the OP values obtained from different acellular assays. On one hand, different transition metals are very sensitive to some OP tests; thus, Cu is very sensitive to OP-DTT, OP-AA, and OP-DCFH assays (Bates et al., 2019; Guo et al., 2020; Molina et al., 2020), while Fe is also a driver of OP-AA but not of OP-DTT (Charrier and Anastasio, 2012; Gao et al., 2020a). However, Mn is not sensitive to AA, but it is very active as catalyst of DTT oxidation in the presence of dissolved oxygen (Charrier et al., 2016; Gao et al., 2020a). On the other hand, some organic compounds are also drivers of PM OP; thus, overall carbonaceous compounds such as elemental carbon (EC), organic carbon (OC), water-soluble organic compounds (WSOC), and aged secondary organic aerosols (SOA) have been associated to OP in the literature (Guo et al., 2020; Pietrogrande et al., 2019; Taghvaee et al., 2019). In addition, organic micropollutants, such as polycyclic aromatic hydrocarbons (PAHs) and quinones are also associated to OP (Bates et al., 2019; Hedayat et al., 2015; Perrone et al., 2016).

Since the chemical composition of ambient PM is associated with its emission sources, some studies are focused on the contribution of PM sources to the OP values measured by different assays (Cesari et al., 2019; Grange et al., 2022; in't Veld et al., 2023; Moufarrej et al., 2020; Taghvaee et al., 2019; Weber et al., 2021). Two methods to estimate the source apportionment of PM OP have been applied in the literature (Weber et al., 2021): (i) by conducting a source attribution method to the PM components to identify the main principal components/factors, and then, using these factors (sources) as input variables to predict OP by means of multilinear regression (MLR) models (Bates et al., 2015; Cesari et al., 2019; Daellenbach et al., 2020; Paraskevopoulou et al., 2019; Verma et al., 2015; Weber et al., 2018, 2021), or by machine learning regression tools (e.g. random forest), that account for the non-linear relationships between the PM chemical composition and sources and their OP (Li et al., 2024), or (ii) by including the OP together with PM composition data as input variables for the source apportionment method (Cesari et al., 2019; Fang et al., 2016; Ma et al., 2018; Verma et al., 2014).

In this study, we have chosen the latter approach to apportion the main element sources that explain the variability of three OP assays (OP-DTT, OP-AA, and OP-DCFH) in size-segregated PM samples (coarse, $PM_{10\text{-}2.5}$, and fine, $PM_{2.5}$ modes) collected in an urban-industrial mixed area. Our study is focused only on elements characterization because of the elevated metal(loid)s local levels due to the proximity of a ferromanganese production plant. However, a chemical/size fractionation approach (Canepari et al., 2019; Massimi et al., 2022) was used to improve the selectivity of the elements as source tracers, as the soluble (in a phosphate buffer aqueous solution) and insoluble fractions of most elements in fine and coarse PM are selectively released from different sources. Element concentrations in both fractions of $PM_{10\text{-}2.5}$ and $PM_{2.5}$ are determined. Particular emphasis is placed on Mn levels and their relation with OP, because it is usually a major contributor to OP (Gao et al., 2020a), but, to our knowledge, the sensitivity of OP assays to PM-bound Mn in areas with high ambient Mn levels has not been studied so far.

2. Methods

2.1. PM sampling

The study area was located in Santander Bay, where industrial emissions of metal(loid)s lead to elevated levels of airborne Mn and Fe (Hernández-Pellón and Fernández-Olmo, 2019a, 2019b). A ferromanganese alloy production plant was previously identified as the main metal(loid)s emitter (Otero-Pregigueiro et al., 2018), although other industrial sources are also located in the area, such as a non-integrated steel plant. The production rate of the ferromanganese plant is usually higher than 100,000 tons/year, but during the sampling period, only one out of four furnaces was working.

Sampling was conducted in two sites. The first site was an urban-industrial mixed site located in the southern part of Santander Bay, specifically in Maliaño a 23,000 inhabitants town, on the rooftop of the "Cultural Center of La Vidriera" (latitude: 43º 24' 55.59" N; longitude: 3º 50' 28.48" W) some 450 m north-west of the active furnace of the Mn alloy production plant (Fig. 1). According to our earlier studies, this site is located downwind of the ferromanganese alloy plant (Otero-Pregigueiro et al., 2018; Hernández-Pellón and Fernández-Olmo, 2019a). A more detailed description of this sampling site is found in Hernández-Pellón and Fernández-Olmo (2019a,b).

The second site was an urban background site located in northern Santander. Specifically, it was situated on the rooftop of the Engineering School (ETSIIT) of the University of Cantabria (latitude: 43º 28' 22.43" N; longitude: 3º 47' 53.31" W); in this site, the influence of the industrial emissions is much lower than in the Vidriera site.

Size-segregated PM samples ($PM_{10\text{-}2.5}$ and $PM_{2.5}$ filters) were collected using an impactor (Dekati® PM_{10} Impactor, PM2530) with a flow rate of 30 L/min for 24 h on 25 and 47 mm-diameter polycarbonate and Teflon filters, respectively. Two samples per week (one on weekdays and one on weekends) were taken. Overall, 38 filters (19 $PM_{10\text{-}2.5}$ and 19 $PM_{2.5}$ daily filters) were collected at the Vidriera site, from January 25th to March 29^{th,} 2023; at the ETSIIT site, 20 filters (10 $PM_{10\text{-}2.5}$ and 10 $PM_{2.5}$ daily filters) were collected, from May 21st to June 21^{st,} 2023.

Teflon $PM_{2.5}$ filters were weighed before and after sampling under controlled temperature and relative humidity conditions using an analytical balance (Sartorious, M-pact AX4202), while a microbalance (Sartorius MCE10.6S-2S00-M Cubis-II) was used for $PM_{10\text{-}2.5}$ filters. Then, they were stored in Petri dishes in a freezer (CryoCube® F101h) at −50 °C. The filters were cut into two pieces using ceramic scissors; half of the filter was used for the OP-DTT and OP-AA analyses, while the other half was used for the OP-DCFH analysis and for the determination of the soluble and insoluble element concentrations.

2.2. PM chemical characterization

The chemical fractionation procedure for the analysis of elements in the soluble and insoluble fractions of PM collected on membrane filters is extensively detailed in Canepari et al. (2009) and in Massimi et al. (2022) and was modified by performing the extraction in phosphate buffer (PB) instead of deionized water. Briefly, each half-filter was extracted in 5 mL of a 0.01 M aqueous solution of PB under rotating agitation (Rotator, Glas-Col, USA) at 30 rpm for 24 h. Then, the solutions were filtered on a nitrocellulose membrane filter (NC Millipore, pore size 0.45 μm, Billerina, MA, EE.UU.) and split into two aliquots. The first aliquot was acidified by ultrapure HNO_3 (65 %, RPE, Carlo Erba, Rome, Italy) to achieve a sample acidity of 2 % and pH < 1, which is equal to that of the standard solutions used for the calibration lines, and then used for the determination of the concentration of 39 elements (Al, As, B,

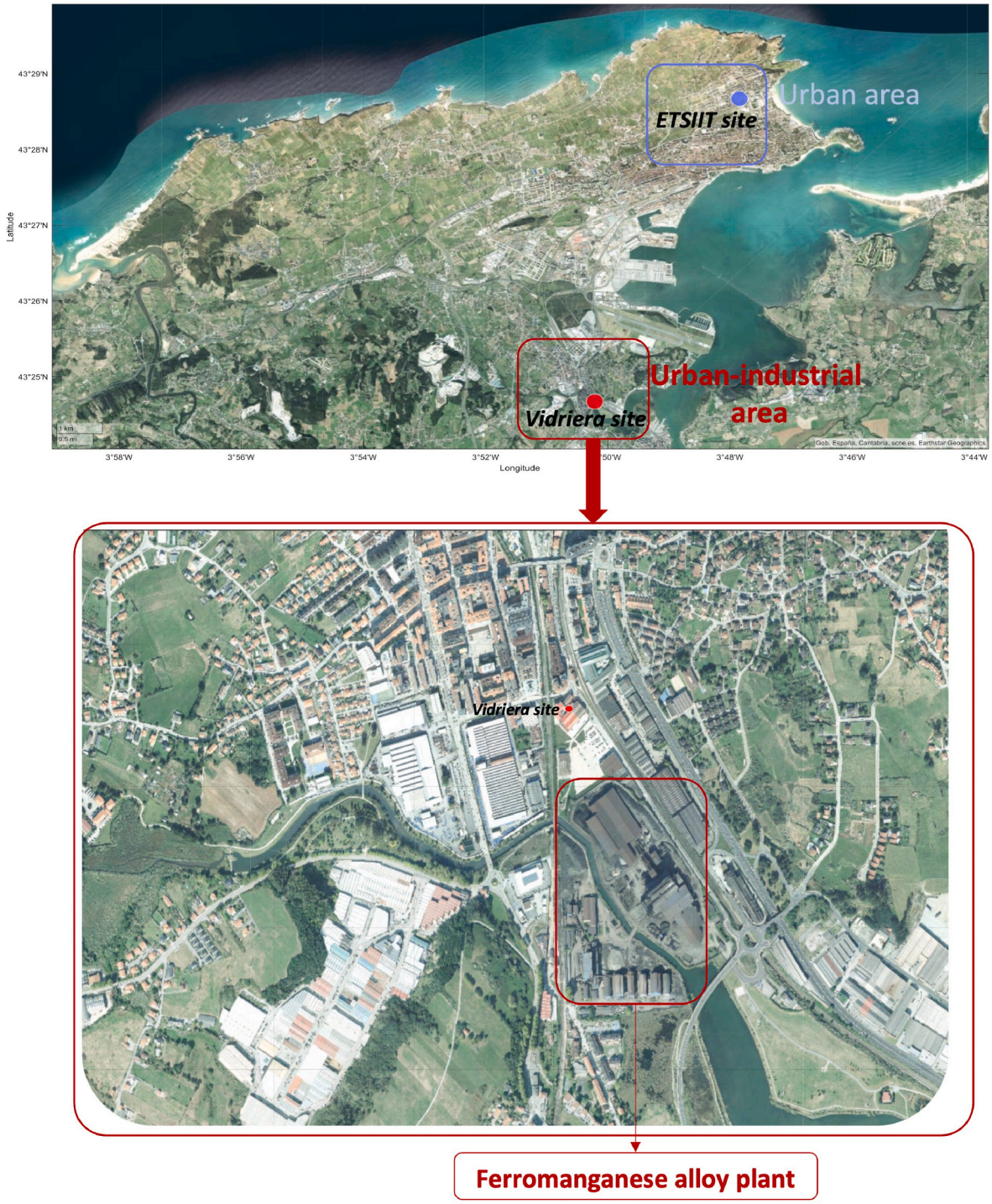

Fig. 1. Location of the sampling sites and the ferromanganese alloy production plant.

Ba, Be, Bi, Ca, Cd, Ce, Co, Cr, Cs, Cu, Fe, Ga, K, La, Li, Mg, Mn, Mo, Na, Nb, Ni, P, Pb, Rb, Sb, Se, Sn, Sr, Te, Ti, Tl, U, V, W, Zn y Zr) in the PB-soluble fraction of $PM_{2.5}$ and $PM_{10\text{-}2.5}$ by a quadrupole inductively coupled plasma-mass spectrometer (ICP-MS, Bruker 820-MS, Billerica, MA, EE.UU) equipped with a glass nebulizer (0.4 mL min^{-1}; Analytik Jena AG, Jena, Germany) and an interference abatement reaction cell. The external standard calibration curve for each element was performed by serially diluting standard stock solutions (1000 ± 2 mg L^{-1}; Exaxol Italia Chemical Manufacturers Srl, Genoa, Italy; Ultra Scientific, North Kingstown, RI, USA; Merck Millipore Ltd., Billerica, MA, USA) in the range 1–500 μg L^{-1}. Yttrium (1000 ± 2 mg L^{-1}; Panreac Qumica, Barcelona, Spain) was used as an internal standard for all measurements to control nebulizer efficiency. The instrumental conditions and performance of the method were according to Canepari et al. (2009). The remaining solution was used for the DCFH assay.

The $PM_{2.5}$ and $PM_{10\text{-}2.5}$ half filter containing the residue and the nitrocellulose membrane filter (insoluble fraction) were subjected to microwave-assisted acid digestion using HNO_3/H_2O_2 (2:1) mixture. The digestion solutions were then diluted with ultrapure water (1:25) to achieve a sample acidity of 2% and filtered through syringe filters (25 mm diameter, 0.45 μm pore size, GVS Filter Technology, Morecambe, England, UK). Finally, the insoluble fractions of $PM_{2.5}$ and $PM_{10\text{-}2.5}$

samples were analyzed by ICP-MS for the same elements present in the soluble fraction. The limits of detection (LOD) of the measured elements and the percentage of data above the LOD are given in the supplementary material (see Table S1), for both the PB-soluble and insoluble fractions. PM samples (soluble and insoluble fraction) were stored at −20 °C until their analysis.

Both, PB-soluble and insoluble element concentrations were expressed as ng/m^3, from their aqueous concentration (ng/mL) multiplied by the liquid volume (mL) and divided by the volume of collected air (m^3).

2.3. Oxidative potential assays

Three OP assays were conducted in the soluble fraction of $PM_{10-2.5}$ and $PM_{2.5}$ filters: OP-DTT, OP-AA, and OP-DCFH. For the OP-DTT and OP-AA assays, the first half of each filter was extracted with 5 mL of a phosphate buffer aqueous solution (0.01 M) in an end-over-end rotation incubator system for 24h at 30 rpm and at 37 ° C using 15 mL polypropylene (PP) tubes. After the extraction, the supernatants were filtered through a 0.45 μm polypropylene syringe filter (25 mm, GVS Filter Technology, Morecambe, United Kingdom). The samples were stored until analysis at 4 ° C and the maximum storage time was 24h.

OP-AA, expressed firstly as μM/min, was determined from the AA depletion curves (AA concentration versus time) by considering the slope of the linear part of the curve. The ascorbate concentration was measured by using a UV/VIS microplate reader (Multiskan SkyHigh microplate spectrophotometer, Thermo Fisher Scientific) and 96 well plates with UV-transparent flat bottoms (Thermo Scientific™ 8404). In each well of the plate, 160 μL of the PM extract was placed, and it was incubated at 37 °*C* for 5 min with continuous high shaking. Then, 40 μL of AA solution (1 mM prepared in ultrapure water) was added to the wells, and the absorbance of ascorbate was measured at 265 nm in each well every 2min for 2h at 37 °*C* with continuous high shaking.

Similarly, OP-DTT was determined with the same microplate reader spectrophotometer, using 96 well-black plates with a clear flat bottom (Corning™ 3904). In each well of the plate, 160 μL of the PM extract was incubated at 37 °*C* for 5 min under continuous high shaking. Then, 25 μL of a DTT solution (0.8 mM prepared in PB 0.01M) was added to the wells, and finally, at selected reaction times (10, 20, 30, and 40 min), 15 μL of DTNB (3 mM prepared in PB 0.01M) was incorporated to form 2-nitro-5-thiobenzoic acid (TNB). After 10 min of the addition of DTNB, the absorbance of mercaptide ion (TNB^{2-}) was measured at 412 nm. More details on OP-AA and OP-DTT assays can be found in Expósito et al. (2024).

In both assays, absorbance was transformed to AA or DTT concentration using a calibration curve with five known AA or DTT concentrations in PB 0.01 M. Measurements were made in triplicate (RSD<7%) and were blank-corrected. Finally, OP-AA and OP-DTT were expressed as nmol/min/m^3 and pmol/min/μg.

OP-DCFH analysis was performed on the same day of the extraction. The OP-DCFH procedure was based on the Simonetti et al. (2018) study. In brief, 1.5 ml of each PM extract was mixed with 5 ml of horseradish peroxidase (HRP) (0.5 units mL^{-1}) and 125 μL of a DCF-DA solution previously activated with NaOH 0.01M. After a 15 min incubation period at 37 °*C*, the oxidation of DCFH was measured through the emitted radiation at 530 nm (excitation wavelength 427 nm) from 2', 7′-diclorofluorescecein (DCF) by a fluorescence detector (Jasco FP-920). A daily calibration curve was obtained by using standard H_2O_2 solutions to convert fluorescence intensity into molar equivalents of H_2O_2 (M H_2O_2), after which the average filter blanks were subtracted. Then, the results were expressed in nmol H_2O_2 equivalent per sampled volume (nmol H_2O_2 eq/m^3) or per sample mass (nmol H_2O_2 eq/μg).

2.4. Statistical analyses

Statistical analysis of the data was performed using IBM SPSS Statistics software (version 22). Relationships between the three OP assays and soluble concentrations of elements were investigated by calculating correlation coefficients. Since, according to the Kolmogorov-Smirnov test, most distributions deviated from the normality, the association between element concentrations and OP values was evaluated by determining the Spearman correlation coefficients (rho). To establish statistical significance a probability level of $p < 0.05$ was chosen.

In addition, a source apportionment analysis, considering only the soluble concentration of those elements with more than 50 % of data above the LOD, and OP-DTTv, OP-AAv, and OP-DCFHv in both size fractions, was carried out. This approach was only applied to the Vidriera dataset to assess the variance contribution of industrial emissions to the OP values measured near the ferromanganese alloy plant. Principal Component Analysis (PCA) was applied since it can combine in the same dataset not only composition-type variables but other related variables such as OP. Before applying the PCA, data was first transformed into a dimensionless standardized form to consider the data set variability using the following equation:

$$Z = \frac{x - X}{\alpha} \quad (1)$$

where x is the daily concentration of the element (soluble fraction) or OP-AAv, OP-DTTv, or OP-DCFHv, X is the arithmetic mean and α is the standard deviation. Varimax orthogonal rotation was performed on the resolved factors to facilitate the interpretation. Resolved factors with high eigenvalues compared to the unity were considered. Additionally, the Kaiser-Meyer-Olkin (KMO) value was above 0.6 and the Bartlett value was found to be significant ($p < 0.01$).

3. Results and discussion

3.1. Levels of PM and elements in coarse and fine size fractions

The concentrations of elements in the soluble fraction of $PM_{10-2.5}$ and $PM_{2.5}$ samples at the urban-industrial mixed site are shown in Table 1, together with the levels found at the urban site (ETSIIT). The concentration of these elements in the insoluble fraction is shown in Table S2. The mass concentration of $PM_{10-2.5}$ and $PM_{2.5}$ is shown in Table S3. The $PM_{10-2.5}$ mass concentration was slightly higher in the urban site than in the urban-industrial mixed site, whereas the $PM_{2.5}$ mass concentration was slightly lower. The sum of the coarse and fine fractions was very similar at both sites (21.2 (urban-industrial) vs 20.9 (urban) μg/m^3).

However, elemental profiles were quite different at both sites. In particular, the concentration of the insoluble Mn, Fe, and Pb in both particle size modes was much higher at the Vidriera site, located near the ferromanganese alloy plant: the insoluble concentrations were 212 and 591 ng/m^3 for Fe, 127 and 540 ng/m^3 for Mn and 1.71 and 0.94 ng/m^3 for Pb in the coarse and fine modes, respectively, at the urban-industrial site, while at the urban site they were 21.9 and 19.1 ng/m^3 for Fe, <LOD and 0.3 ng/m^3 for Mn and 0.04 and 0.15 ng/m^3 for Pb. However, in the soluble fraction, although the concentration of Mn and Pb was higher in the urban-industrial site (14.2 and 51.2 ng/m^3 for Mn at the urban-industrial site in the coarse and fine modes, respectively, vs 1.06 and 1.76 ng/m^3 at the urban site; and 0.13 and 1.39 ng/m^3 for Pb at the urban-industrial site in the coarse and fine modes, respectively, vs 0.023 and 0.64 ng/m^3 at the urban site), the concentration of Fe in the urban site was higher (8.06 and 16.5 ng/m^3 at the urban site vs 2.77 and 8.63 ng/m^3 near the industrial source, in the coarse and fine modes, respectively). This was attributed to the very low solubility of Fe in ferromanganese and silicomanganese particles emitted from the alloy plant.

The total average level of Mn at this site was 764 ng/m^3 (see Table S2); this value was similar to that found by Hernández-Pellón and Fernández-Olmo (2019b) in 2015 (722 ng/m^3) at the same site. However, in 2015, the four electric furnaces of the ferromanganese refinery

Table 1
The soluble concentration of the studied elements (ng/m^3) in both $PM_{10-2.5}$ and $PM_{2.5}$ fractions at the urban-industrial mixed site (Vidriera) and the urban site (ETSIIT).

	Urban-industrial area				Urban area			
	$PM_{10-2.5}$		$PM_{2.5}$		$PM_{10-2.5}$		$PM_{2.5}$	
Elements	Mean	SD	Mean	SD	Mean	SD	Mean	SD
Al	2.4	3.64	5.59	3.92	1.35	0.91	2.12	2.44
As	>50% <D.L.		0.18	0.13	>50% <D.L.		0.11	0.073
B	>50% <D.L.		1.47	1.15	>50% <D.L.		0.94	0.74
Bi	0.015	0.012	0.11	0.14	0.004	0.0036	0.078	0.089
Ca	80.5	57.6	113	55.9	67.7	44.1	34.1	26.5
Cd	0.035	0.029	0.17	0.12	>50% <D.L.		>50% <D.L.	
Ce	>50% <D.L.		0.07	0.067	0.030	0.0249	0.056	0.039
Co	0.096	0.065	0.34	0.24	0.021	0.0125	0.047	0.022
Cr	>50% <D.L.		0.26	0.16	>50% <D.L.		0.121	0.090
Cs	0.002	0.001	0.026	0.039	>50% <D.L.		0.013	0.018
Cu	>50% <D.L.		0.95	0.57	>50% <D.L.		0.90	1.11
Fe	2.77	3.05	8.63	8.1	8.06	8.76	16.5	16.1
K	22	12.1	105	67.3	22.6	14.2	49.0	46.3
La	>50% <D.L.		0.008	0.006	>50% <D.L.		0.007	0.005
Li	0.046	0.033	0.13	0.086	0.012	0.0063	0.021	0.013
Mg	27.5	22.5	45.1	60	29.5	9.64	30.2	13.7
Mn	14.2	19.2	51.2	57.7	1.06	0.88	1.76	1.10
Mo	>50% <D.L.		0.18	0.17	>50% <D.L.		0.13	0.13
Nb	>50% <D.L.		0.071	0.046	>50% <D.L.		0.033	0.051
Ni	>50% <D.L.		0.3	0.12	>50% <D.L.		0.22	0.056
Pb	0.13	0.18	1.39	1.8	0.023	0.0253	0.64	0.92
Rb	0.037	0.016	0.32	0.34	0.021	0.0244	0.076	0.055
Sb	0.019	0.007	0.3	0.31	0.015	0.0074	0.22	0.19
Se	0.024	0.014	0.23	0.26	>50% <D.L.		0.31	0.21
Sn	0.006	0.002	0.11	0.13	0.051	0.0493	0.16	0.14
Sr	0.43	0.27	0.64	0.4	0.35	0.14	0.26	0.16
Te	>50% <D.L.		0.016	0.015	>50% <D.L.		>50% <D.L.	
Tl	0.013	0.009	0.092	0.12	0.014	0.0135	0.20	0.24
V	0.036	0.018	0.21	0.11	0.021	0.0138	0.39	0.17
W	0.007	0.004	0.019	0.009	0.005	0.0091	>50% <D.L.	
Zn	2.5	1.76	14	10.7	>50% <D.L.		20.0	18.2

were working, whereas only one furnace was active in the current sampling campaign. The measured Mn level is clearly higher than the annual guideline for airborne Mn recommended by the WHO (150 ng/m^3).

The distribution of elements and total mass concentration between $PM_{2.5}$ and PM_{10} is shown in Fig. S1 for those elements with more than 50 % of data above the LOD. In the urban-industrial site, the fraction of elements in the fine mode is higher than in the urban site; in particular, the $PM_{2.5}/PM_{10}$ ratio for most elements is higher than 0.75, except for crustal elements (Al, Ca), and those elements enriched in marine aerosols (Mg, K). In the urban site, the $PM_{2.5}/PM_{10}$ ratio of Al, Ca, Fe, K, Mg, Mn, and Sn was lower, while the ratio of Pb, Sb, and V was similar and even higher than that of the urban-industrial site.

The concentration of Cu, Fe, and Mn, the three most active transition metals in OP assays, in the soluble fraction is low with respect to their total content, mainly in the coarse mode (>50 % of samples showed soluble Cu concentration in $PM_{10-2.5}$ below the LOD), because of their low solubility in PB. Phosphate-based metals solubilities lower than 10 %, mainly for Fe, were reported by Ghanem et al. (2021) from welding fumes reference materials. The PB-solubilities of metals found in this work were clearly lower than those found in the same site (Santander bay) and the same season (winter) for Hernández-Pellón et al. (2018) in artificial lysosomal fluid (ALF) and Gamble's solution, two widely used synthetic lung fluids. Similar results were also obtained from Pelfrêne et al. (2017), who reported lower solubilities of some trace metals in saline PB (PBS) than in Gamble's solution and ALF. Since the determination of PM OP requires a preliminary extraction step before measuring the antioxidant depletion, the use of a relatively simple extraction solution is recommended, such as a PB solution, as usually reported in the literature.

3.2. Oxidative potential

Fig. 2 shows the box plots of the OPv values (OP-DTT, OP-AA, and OP-DCFH) in both $PM_{10-2.5}$ and $PM_{2.5}$ samples measured at the urban-industrial mixed site (Vidriera) and the urban site (ETSIIT). Although similar mass concentrations of $PM_{10-2.5}$ and $PM_{2.5}$ were obtained at both sites, the OPv values are quite different, much higher at the urban-industrial site for the three OP assays (see Table S3 and Fig. 2). The differences in the composition of coarse and fine PM between the two sites explain the variability found in OP values. This is clearly observed for Mn, one of the main drivers of OP-DTT and OP-DCFH, which shows a much higher concentration in the urban-industrial mixed site, due to its proximity to the ferromanganese alloy plant. However, in the case of OP-AA, since Mn is not a driver of this assay (Expósito et al., 2024), and the levels of Cu and Fe are similar and even lower than in the urban site, other drivers could explain the higher OP-AA values found in the urban-industrial site; it is suggested that a higher organic content at the urban-industrial site would have led to higher OP-AA values (coke is used as reducer in the electric furnaces of the ferromanganese alloy plant).

When OP values were normalized by PM mass the average OP-DTTm and OP-AAm were similar for the two particle size fractions at both sites, except for OP-DTT in the urban area, with a higher mass value in the coarse fraction (see Table S3). In the case of OP-DCFHm, a much higher OP value was found for the coarse fraction at both sites, showing the importance of the most sensitive active metal species present in the coarse fraction (Massimi et al., 2020; Perrone et al., 2016).

The OP-DTTv and OP-AAv values obtained in this work are compared with those reported in the literature measured at other sites in Europe (see Table 2). This comparison has been made only for $PM_{2.5}$ because most OP assays are applied to this size fraction. The mean OP-DTTv value obtained in the urban-industrial mixed site (0.38 nmol/min/m^3) is within the values found in the literature for European sites;

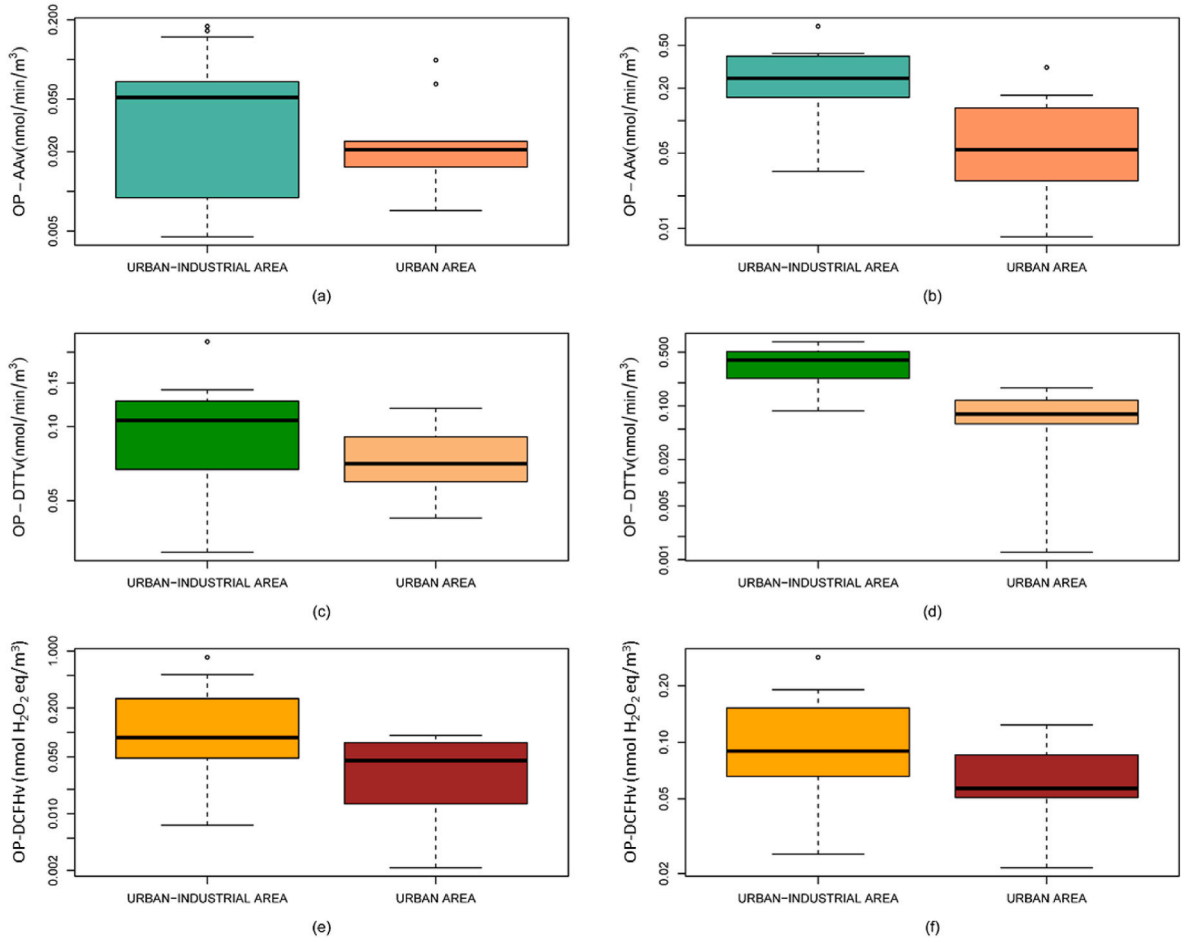

Fig. 2. Box plots of OP-DTTv, OP-AAv, and OP-DCFHv in $PM_{10-2.5}$ (a, c, e) and $PM_{2.5}$ (b, d, f) samples at the urban-industrial mixed site (Vidriera, n = 19) and the urban site (ETSIIT, n = 10).
* The ends of the boxes, and the line across each box represent the 25th and 75th percentiles, and the median, respectively; the upper and lower whiskers represent Q3 ±1.5xIQR; open circles indicate data outliers.

however, at the urban site, the mean value (0.083 nmol/min/m^3) was lower than that found in many European urban sites; only, the work of Jedynska et al. (2017) in Oslo (Norway), London (UK), and Helsinki (Finland), reported similar results: 0.13, 0.14, and 0.15 nmol/min/m^3, respectively, but they used ethanol to extract the $PM_{2.5}$ filters.

Regarding the OP-AA assay, the mean value obtained in the urban-industrial mixed site (0.28 nmol/min/m^3) was slightly lower than that found in other European studies (Grange et al., 2022; in't Veld et al., 2023). The mean value at the urban site (0.089) was lower than that reported in European sites.

Regarding the comparison of OP-DCFHv, there has been limited investigation into the measured OP-DCFHv of $PM_{2.5}$ samples in Europe. Jovanovic et al. (2019) found significantly higher values of OP-DCFHv in $PM_{2.5}$ samples in Belgrade (Serbia) (3.14 nmol H_2O_2 eq/m^3) than the values obtained in this study (0.11 and 0.065 nmol H_2O_2 eq/m^3 in urban and industrial area, respectively). However, $PM_{2.5}$ samples were collected near a tunnel with heavy traffic, which can explain the high OP-DCFH values found in Jovanovic et al. work. Out of Europe, a wide range of OP-DCFH values was found by Khurshid et al. (2014) in Austin (Texas, US) (from 0.02 to 3.81 nmol H_2O_2 eq/m^3), with lower values in winter. Campbell et al. (2021) reported low values in the urban area of Beijing (China) (mean value in summer of 0.17 nmol H_2O_2/m^3).

3.3. Correlation of oxidative potential values with the concentration of elements in PM

A deeper analysis of the association between OP and PM composition has been made at the Vidriera site, because of the characteristics of the composition profile of PM near the ferromanganese alloy plant. Table 3 shows the Spearman correlation coefficients obtained for OP-DTTv, OP-AAv, and OP-DCFHv with the soluble element concentrations in both size fractions, $PM_{10-2.5}$ and $PM_{2.5}$. The intercorrelations between the OPv assays measured in both size fractions are also shown in Table 4.

OP-DTTv and OP-DCFHv are highly correlated in the coarse fraction (0.76) and moderately correlated in the fine fraction (0.57), due to the high correlation of soluble Mn with both OP assays, mainly in the coarse fraction (0.85 and 0.93 for OP-DCFH and OP-DTT, respectively). This leads to relatively high correlation coefficients between the fine and coarse fractions of OP-DTTv (0.72) and OP-DCFHv (0.62), as shown in Table 4. However, no correlation was found between OP-AA in coarse and fine fractions. In fact, none of the studied elements in the soluble fraction were correlated with OP-AA in $PM_{2.5}$, while Al, Mn, and Sb showed moderate correlation coefficients in the coarse fraction, leading to a moderate correlation between OP-AAv and OP-DTTv. Therefore, whereas the same elements were active in the fine and coarse fractions for OP-DTT and OP-DCFH, the elements active in the OP-AA assay varied with the particle size (see Table 3), as suggested in the literature (Perrone et al., 2019; Simonetti et al., 2018; Massimi et al., 2020). Surprisingly, OP-AAv was moderately correlated with both OP-DTTv

Table 2
Comparison of measured OPv values in $PM_{2.5}$ with other sites in Europe.

References	Place	Country	Area	Leaching agent	Mean $PM_{2.5}$ (μg/m^3)	Mean OP-DTTv (nmol/min/m^3)	Mean OP-AAv (nmol/min/m^3)	Mean OP-DCFHv (nmol H_2O_2/m^3)
This study	Cantabria	Spain	Urban-industrial	PB	16.6	0.38	0.28	0.11
			Urban		14.5	0.083	0.089	0.064
Pietrogrande et al. (2022)	Milan	Italy	Urban background	PB	18.2	0.21	0.52	
Pietrogrande et al. (2021)	Po Valley	Italy	Urban-rural			0.19	0.38	
				Gamble		0.10	0.34	
				Methanol		0.11	0.22	
In't Veld et al. (2023)	Barcelona	Spain	Urban background	Gamble +		1.20	1.00	
	Montseny		Rural background	DPPC		0.40	0.30	
Grange et al. (2022)	Bern-Bollwerk	Switzerland	Traffic urban			1.10	1.60	
	Zürich-Kaserne		Urban			0.80	0.80	
	Basel-Binningen		Suburban			0.60	0.70	
	Magadino-Cadenazzo		Rural			0.70	1.20	
	Payerne		Rural			0.60	0.40	
Moufarrej et al. (2020)	Dunkerque	France	Industrial	Gamble	29.2	0.36	1.12	
Jovanovic et al. (2019)	Belgrade	Serbia	Traffic urban	Water		0.37		3.14
Cesari et al. (2019)	Campania	Italy	Urban-industrial	Water	16.3	0.19		
Chirizzi et al. (2017)	Lecce	Italy	Urban background		31.9	0.40		
Giannossa et al. (2022)	Lecce	Italy	Urban background		18.0	0.29		
Jedynska et al. (2017)	Oslo	Norway	Multisite: Regional	Ethanol		0.13		
	Helsinki/Turku	Finland	background, urban			0.15		
	Copenhagen	Denmark	background, street			0.21		
	London/Oxford	U.K.				0.14		
	Rotterdam, Amsterdam, Groningen, Amersfoort	Netherlands				0.20		
	Munich/Augsburg	Germany				0.20		
	Paris	France				0.23		
	Catalonia	Spain				0.23		
	Rome	Italy				0.23		
	Athens	Greece				0.28		

(0.53) and OP-DCFHv (0.50) in the fine fraction.

No consensus about the associations between these OP assays has been found in the literature; thus, some authors reported that OP-DTT and OP-DCFH assays are well correlated, but OP-AA is sensitive to other PM species (Massimi et al., 2020; Simonetti et al., 2018). However, other references have reported high/moderate associations between OP-AA and OP-DTT (Calas et al., 2018; Campbell et al., 2021; Fadel et al., 2023; Gao et al., 2020b) as well as between OP-AA and OP-DCFH (Campbell et al., 2021; Dominutti et al., 2023).

3.4. Sources of elements and associated oxidative potential near the ferromanganese alloy plant

To clarify the association between the PM soluble elements in both size fractions and their sources with the OPv values obtained from the three OP assays, a PCA was performed on the Vidriera dataset. The results obtained from this PCA after VARIMAX rotation are shown in Fig. 3; factor loadings higher than 0.7 are depicted in red color. Four principal components (PCs) or factors have been included, explaining 65 % of the total variance:

(i) The first PC was attributed to road traffic emissions, accounting for 21.1 % of the explained variance. Among the typical tracers of road traffic, Cu, Fe, and Zn in the soluble fraction of the fine mode presented high factor loadings (>0.7). Antimony, other important tracer of road traffic emission also presented a moderate factor loading in the soluble fine fraction, but of lower magnitude (0.40). Copper and Fe are usually found in brake pads (Charron et al., 2019; Gonet and Maher, 2019) together with Sb. However, during the last decade, the introduction of Sb-free brake pads has led to lower Sb emissions and therefore, lower levels of airborne Sb (Charron et al., 2019), thus explaining the relatively low factor loading found in our work. In addition, Zn has been proposed as a key tracer of tire wear emissions, since it is one of the most abundant metallic elements in tires commercialized in the US and EU (Apeagyei et al., 2011; Pant and Harrison, 2013). In addition, the fairly high factor loading found for soluble K in the fine mode (0.77), typically associated with emissions from biomass combustion (Canepari et al., 2019; Massimi et al., 2020, 2022; Simonetti et al., 2018) suggests that other urban sources related to domestic biomass heating cannot be ruled out within this factor. The loadings of OP in this factor are low: 0.46 and 0.27 for OP-DTT in the coarse and fine modes, respectively, and even lower for OP-AA; although Cu is the best tracer of OP-AA and OP-DTT assays (Bates et al., 2019; Guo et al., 2020), since the solubility of Cu in PB was very low, small factor loadings for OP-DTT and OP-AA were obtained.

(ii) PC2 was assigned to the ferromanganese alloy plant and accounts for 18.9 % of the variance. It is clearly the main factor associated with OPv values, mainly to OP-DTT and OP-DCFH in the coarse fraction (factor loadings of 0.74 and 0.94, respectively). The OP-DTT in the fine mode also presents a relatively high factor loading (0.61). This factor is mainly characterized by the presence of soluble Mn in both particle size fractions, with factor loadings close to 0.90 for both cases. Our results support that Mn is the best tracer of ferromanganese refineries, as previously reported in the literature (Haynes et al., 2012; Hernández-Pellón and Fernández-Olmo, 2019a). Manganese is also one of the main drivers of

Table 3
Spearman correlations between the concentration of soluble elements and OP assays: (a) $PM_{10\text{-}2.5}$; (b) $PM_{2.5}$.

Elements (ng/m^3)	OP-DCFHv (nmol H_2O_2 eq/m^3)	OP-DTTv (nmol/min/m^3)	OP-AAv (nmol/min/m^3)
(a)			
Al_s	0.34	**0.48**	**0.54**
Bi_s	0.39	0.20	−0.14
Ca_s	0.26	0.37	0.44
Cd_s	0.26	0.25	0.08
Co_s	0.32	0.32	0.09
Cs_s	**0.84**	**0.76**	0.35
Fe_s	−0.13	0.11	0.39
K_s	0.07	−0.20	0.02
Li_s	0.09	−0.08	−0.24
Mg_s	−0.24	−0.23	−0.17
Mn_s	**0.85**	**0.93**	**0.47**
Pb_s	0.23	0.09	0.09
Rb_s	0.43	0.34	0.45
Sb_s	0.07	0.45	**0.46**
Se_s	−0.39	**−0.55**	−0.19
Sn_s	−0.35	−0.01	0.42
Sr_s	0.27	0.16	0.19
Tl_s	0.29	0.15	−0.22
V_s	0.14	0.22	0.23
W_s	0.17	0.13	0.06
Zn_s	0.15	0.20	0.45
(b)			
Al_s	−0.13	0.17	−0.23
As_s	0.23	**0.59**	0.26
B_s	0.06	0.44	0.01
Bi_s	0.21	**0.68**	0.11
Ca_s	−0.11	−0.10	−0.23
Cd_s	0.20	**0.61**	0.12
Ce_s	0.00	0.39	0.13
Co_s	0.30	**0.82**	0.28
Cr_s	0.02	**0.55**	0.39
Cs_s	0.40	**0.77**	0.13
Cu_s	0.18	**0.56**	0.29
Fe_s	−0.05	0.35	0.18
K_s	0.32	**0.66**	0.07
La_s	0.04	0.41	0.12
Li_s	0.33	**0.68**	0.25
Mg_s	0.13	−0.18	0.12
Mn_s	**0.54**	**0.80**	0.18
Mo_s	0.21	0.39	0.23
Nb_s	0.06	−0.18	−0.28
Ni_s	0.14	0.22	0.01
Pb_s	−0.04	0.21	−0.08
Rb_s	0.30	**0.72**	0.08
Sb_s	0.06	**0.52**	0.09
Se_s	0.20	0.22	0.02
Sn_s	−0.03	**0.54**	0.14
Sr_s	−0.04	−0.19	−0.34
Te_s	**0.53**	**0.52**	0.05
Tl_s	0.43	**0.79**	0.20
V_s	−0.12	−0.05	−0.43
W_s	0.11	**0.71**	0.21
Zn_s	0.32	**0.52**	0.22

In **bold**, correlation coefficients with **p-value<0.05**.

Table 4
Spearman intercorrelations between OPv assays (OP-DCFH, OP-DTT, and OP-AA) in both size fractions.

	OP-DCFHv $PM_{10\text{-}2.5}$	OP-DTTv $PM_{10\text{-}2.5}$	OP-AAv $PM_{10\text{-}2.5}$	OP-DCFHv $PM_{2.5}$	OP-DTTv $PM_{2.5}$	OP-AAv $PM_{2.5}$
OP-DCFHv $PM_{10\text{-}2.5}$	1.00					
OP-DTTv $PM_{10\text{-}2.5}$	**0.76**	1.00				
OP-AAv $PM_{10\text{-}2.5}$	0.18	**0.54**	1.00			
OP-DCFHv $PM_{2.5}$	**0.62**	**0.59**	0.21	1.00		
OP-DTTv $PM_{2.5}$	**0.59**	**0.72**	0.39	**0.57**	1.00	
OP-AAv $PM_{2.5}$	−0.03	0.17	0.08	**0.50**	**0.53**	1.00

the OP-DTT assay (Bates et al., 2019; Charrier et al., 2016; Guo et al., 2020); our study also reveals that Mn is a good driver of OP-DCFH, as reported in other studies (Massimi et al., 2020). Rubidium also presented a high factor loading in this PC in the fine fraction, which is attributed to Mn ores impurities. Lead and Zn in the fine fraction were also found in this factor, but with lower loadings (see Fig. 3). Both metals were previously associated with this industrial source (Hernández-Pellón and Fernández-Olmo, 2019a).

(iii) The third PC is attributed to crustal material. Although it explains 14.8 % of the total variance, the factor loadings of OP are practically null (see Fig. 3), in agreement with the literature (Chirizzi et al., 2017; Fadel et al., 2023). The factor loading of the mass concentration of the coarse fraction was relatively high (0.53), in agreement with the coarser size of crustal material and resuspended dust. The main tracers (factor loading higher than 0.7) are Al, Ca and Fe in the coarse mode; Al and Ca in the fine mode also presented moderate factor loadings (0.69 and 0.50, respectively). Aluminum and Fe are usually the main tracers of crustal material reported in the literature (Ledoux et al., 2017; Yu and Cao, 2023). Strontium was also present in the fine mode (factor loading of 0.45), in agreement with White (2008), who reported similar levels of soluble Sr in continental crust and sea salt aerosols.

(iv) The last factor considered in this analysis was associated with sea salt aerosol, explaining 9.7 % of the variance. It is well correlated with the mass concentration of coarse PM (factor loading of 0.74). Among the tracers of sea salt aerosols, Na is the most important one (Chan et al., 2000; Savoie and Prospero, 1980); however, the use of sodium phosphate buffer to extract the PM filters has not allowed quantifying the concentration of soluble Na in the samples. High factor loadings of soluble Mg are found in both fine and coarse modes (0.94 and 0.92, respectively). Magnesium is also considered a major component of fresh (Chan et al., 2000) and aged (Weber et al., 2021) sea salt aerosols; in areas poorly affected by anthropogenic activities, the presence of soluble Mg is almost exclusively due to sea salt aerosols (Savoie and Prospero, 1980). Strontium also showed an intermediate factor loading in the fine soluble fraction (0.58), which is also attributed to sea salt aerosol; in fact, non-crustal Sr is widely recognized as a good predictor of sea salt aerosols (White, 2008). Potassium was not included in this factor, although it has been previously identified as a tracer of sea salt aerosols. However, the existence of other K sources in the area, such as biomass burning, may explain the absence of K in PC4. A moderate factor loading for OP-AA in the coarse fraction can be seen for PC4 (0.30). This may suggest the coexistence of aged sea salts, as reported by Borlaza et al. (2021), who found a considerable contribution of aged sea salts to OP-AA. Weber et al. (2021) suggested that the aggregation of organic compounds within the ageing process of sea salts may occur, which can contribute to OP-AA and OP-DTT.

An important limitation here in the relatively small dataset (19 fine

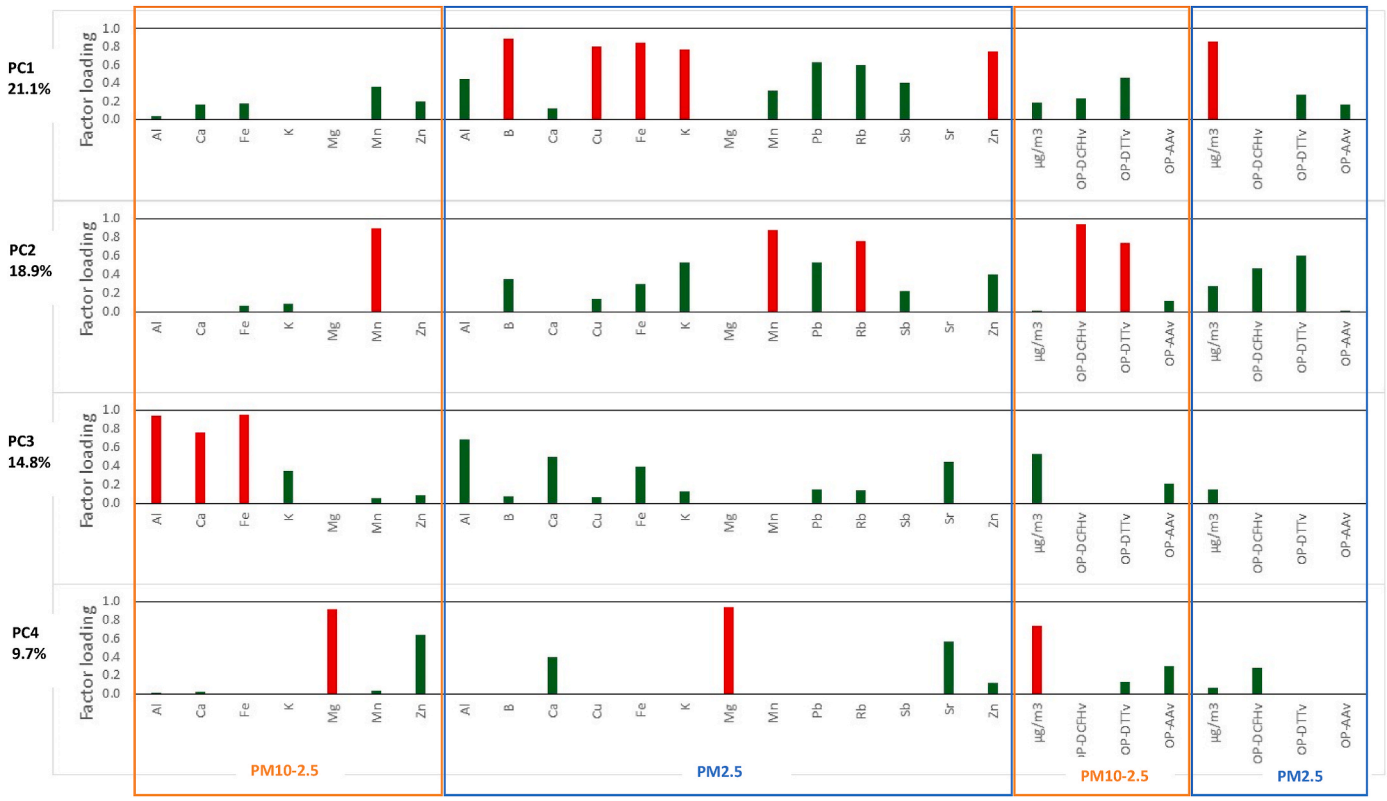

Fig. 3. Factor loadings after VARIMAX rotation from PCA applied to soluble element concentrations and OP-DTTv, OP-AAv, and OP-DCFHv values. Factor loading >0.7 in red color.

and 19 coarse samples), which may limit the generalization ability of PCA. However, the identification of the main tracers of each factor and the attribution of the obtained factors to element sources are similar to those found in former studies in the same study area (Arruti et al., 2010; Hernández Pellón and Fernández-Olmo, 2019a).

4. Conclusion

This study has analyzed three different acellular OP assays (ascorbic acid (AA), dithiothreitol (DTT) and 2,7-dichlorofluorescein (DCFH)) and their sensitivity to the elemental composition of size-segregated PM samples ($PM_{2.5}$, $PM_{10\text{-}2.5}$) collected in an urban-industrial area, mainly characterized by elevated levels of Fe and Mn, due to the proximity of a ferromanganese alloy plant.

The high soluble levels of Mn in both the coarse and fine fractions have led to the high percentage of variance explained of the factor associated to this ferromanganese plant, and to the high factor loadings of OP-DTT and OP-DCFH, since Mn is very active in these OP assays. In contrast, the low solubility of Cu (in phosphate buffer) has led to relatively small factor loadings of OP in the traffic emission factor. Other major elements present in sampled PM confirmed that usual sources of PM mass concentration, such as crustal material and sea salt aerosol, barely affect OP values. Finally, whereas OP-DTT and OP-DCFH were well associated with some of the studied elements and their sources, OP-AA presented the lowest association, mainly because Mn is not a good driver of this assay, and because of the low solubility of Cu and Fe, mainly in the coarse fraction.

CRediT authorship contribution statement

A. Expósito: Writing – review & editing, Software, Investigation. **E. Vaccarella:** Software, Investigation. **L. Massimi:** Writing – review & editing, Data curation. **M. Santibáñez:** Supervision, Funding acquisition. **I. Fernández-Olmo:** Writing – review & editing, Writing – original draft, Supervision, Funding acquisition, Conceptualization.

Funding

This work was supported by the Spanish Ministry of Science and Innovation (Project PID2020-114787RB-I00, funded by MCIN/AEI/10.13039/501100011033 and "ERDF A way of making Europe").

Declaration of competing interest

The authors declare that they have no known competing financial interests or personal relationships that could have appeared to influence the work reported in this paper.

Acknowledgments

We thank Dr. Ana Belén Martin-Arroyo and Lucía Agudo from EVOADAPTA research group for allowing us to use the microbalance (Sartorius MCE10.6S-2S00-M Cubis-II) to weigh the $PM_{10\text{-}2.5}$ filters.

Appendix A. Supplementary data

Supplementary data to this article can be found online at https://doi.org/10.1016/j.apr.2024.102330.

References

Apeagyei, E., Bank, M.S., Spengler, J.D., 2011. Distribution of heavy metals in road dust along an urban-rural gradient in Massachusetts. Atmos. Environ. 45, 2310–2323.

Arruti, A., Fernández-Olmo, I., Irabien, A., 2010. Evaluation of the contribution of local sources to trace metals levels in urban PM2.5 and PM10 in the Cantabria region (Northern Spain). J. Environ. Monit. 12 (7), 1451–1458.

Bates, J.T., Weber, R.J., Abrams, J., Verma, V., Fang, T., Klein, M., Strickland, M.J., Sarnat, S.E., Chang, H.H., Mulholland, J.A., Tolbert, P.E., Russell, A.G., 2015.

Reactive oxygen species generation linked to sources of atmospheric particulate matter and cardiorespiratory effects. Environ. Sci. Technol. 49, 13605–13612.
Bates, J.T., Fang, T., Verma, V., Zeng, L., Weber, R.J., Tolbert, P.E., Abrams, J.Y., Sarnat, S.E., Klein, M., Mulholland, J.A., Russel, A.G., 2019. Review of acellular assays of ambient particulate matter oxidative potential: methods and relationships with composition, sources, and health effects. Environ. Sci. Technol. 53, 4003–4019.
Borlaza, L.J.S., Weber, S., Jaffrezo, J.L., Houdier, S., Slama, R., Rieux, C., Albinet, A., Micallef, S., Trébluchon, C., Uzu, G., 2021. Disparities in particulate matter (PM10) origins and oxidative potential at a city scale (Grenoble, France) - Part 2: sources of PM10 oxidative potential using multiple linear regression analysis and the predictive applicability of multilayer perceptron neural network analysis. Atmos. Chem. Phys. 21 (12), 9719–9739.
Calas, A., Uzu, G., Kelly, F.J., Houdier, S., Martins, J.M.F., Thomas, F., Molton, F., Charron, A., Dunster, C., Oliete, A., Jacob, V., Besombes, J.L., Chevrier, F., Jaffrezo, J.L., 2018. Comparison between five acellular oxidative potential measurement assays performed with detailed chemistry on PM10 samples from the city of Chamonix (France). Atmos. Chem. Phys. 18 (11), 7863–7875.
Campbell, S.J., Wolfer, K., Utinger, B., Westwood, J., Zhang, Z.H., Bukowiecki, N., Steimer, S.S., Vu, T.V., Xu, J., Straw, N., Thomson, S., Elzein, A., Sun, Y., Liu, D., Li, L., Fu, P., Lewis, A.C., Harrison, R.M., Bloss, W.J., et al., 2021. Atmospheric conditions and composition that influence PM2.5 oxidative potential in Beijing, China. Atmos. Chem. Phys. 21 (7), 5549–5573.
Canepari, S., Perrino, C., Astolfi, M.L., Catrambone, M., Perret, D., 2009. Determination of soluble ions and elements in suspended particulate matter: inter-technique comparison of XRF, IC and ICP for sample-by-sample quality control. Talanta 77, 1821–1829.
Canepari, S., Astolfi, M.L., Catrambone, M., Frasca, D., Marcoccia, M., Marcovecchio, F., Massimi, L., Rantica, E., Perrino, C., 2019. A combined chemical/size fractionation approach to study winter/summer variations, ageing and source strength of atmospheric particles. Environ. Pollut. 253, 19–28.
Cesari, D., Merico, E., Grasso, F.M., Decesari, S., Belosi, F., Manarini, F., de Nuntiis, P., Rinaldi, M., Volpi, F., Gambaro, A., Morabito, E., Contini, D., 2019. Source apportionment of PM2.5 and of its oxidative potential in an industrial suburban site in South Italy. Atmosphere 10 (12), 758.
Chan, C.K., Ha, Z., Choi, M.Y., 2000. Study of water activities of aerosols of mixtures of sodium and magnesium salts. Atmos. Environ. 34, 4795–4803.
Charrier, J.G., Anastasio, C., 2012. On dithiothreitol (DTT) as a measure of oxidative potential for ambient particles: evidence for the importance of soluble transition metals. Atmos. Chem. Phys. 12 (5), 11317–11350.
Charrier, J.G., McFall, A.S., Vu, K.K., et al., 2016. A bias in the "mass-normalized" DTT response - an effect of non-linear concentration-response curves for copper and manganese. Atmos. Environ. 144, 325–334.
Charron, A., Polo-Rehn, L., Besombes, J.-L., Golly, B., Buisson, C., Chanut, H., Marchand, N., Guillaud, G., Jaffrezo, J.-L., 2019. Identification and quantification of particulate tracers of exhaust and non-exhaust vehicle emissions. Atmos. Chem. Phys. Discuss. 19, 5187–5207.
Chirizzi, D., Cesari, D., Guascito, M.R., Dinoi, A., Giotta, L., Donateo, A., Contini, D., 2017. Influence of Saharan dust outbreaks and carbon content on oxidative potential of water-soluble fractions of PM2.5 and PM10. Atmos. Env. 163, 1–8.
Cho, A.K., Sioutas, C., Miguel, A.H., Kumagai, Y., Schmitz, D.A., Singh, M., Eiguren-Fernandez, A., Froines, J.R., 2005. Redox activity of airborne particulate matter at different sites in the Los Angeles Basin. Environ. Res. 99, 40–47.
Crobeddu, B., Aragao-Santiago, L., Bui, L.C., Boland, S., Baeza Squiban, A., 2017. Oxidative potential of particulate matter 2.5 as predictive indicator of cellular stress. Environ. Pollut. 230, 125–133.
Daellenbach, K.R., Uzu, G., Jiang, J., Cassagnes, L.-E., Leni, Z., Vlachou, A., Stefenelli, G., Canonaco, F., Weber, S., Segers, A., Kuenen, J.J.P., Schaap, M., Favez, O., Albinet, A., Aksoyoglu, S., Dommen, J., Baltensperger, U., Geiser, M., el Haddad, I., Jaffrezo, J.-L., Prévôt, A.S.H., 2020. Sources of particulate-matter air pollution and its oxidative potential in Europe. Nature 587, 414–419.
Dockery, D.W., Pope, C.A., 1994. Acute respiratory effects of particulate air pollution. Annual Rev. Public Health 15, 107–132.
Dominutti, P.A., Borlaza, L.J.S., Sauvain, J.-J., Ngoc Thuy, V.D., Houdier, S., Suarez, G., Jaffrezo, J.-L., Tobin, S., Trébuchon, C., Socquet, S., Moussu, E., Mary, G., Uzu, G., 2023. Source apportionment of oxidative potential depends on the choice of the assay: insights into 5 protocols comparison and implications for mitigation measures. Environ. Sci.: Atmos. 3, 1497–1512.
European Parliament, 2022. Proposal for a DIRECTIVE OF THE EUROPEAN PARLIAMENT AND OF THE COUNCIL on ambient air quality and cleaner air for Europe (recast). https://eur-lex.europa.eu/legal-content/EN/TXT/?uri=COM%3A2022%3A542%3AFIN. (Accessed 7 September 2023).
Expósito, A., Maillo, J., Uriarte, I., Santibáñez, M., Fernández-Olmo, I., 2024. Kinetics of ascorbate and dithiothreitol oxidation by soluble copper, iron, and manganese, and 1,4-naphthoquinone: influence of the species concentration and the type of fluid. Chemosphere 361, 142435.
Fadel, M., Courcot, D., Delmaire, G., Roussel, G., Afif, C., Ledoux, F., 2023. Source apportionment of PM2.5 oxidative potential in an East Mediterranean site. Sci. Total Environ. 900, 165843.
Fang, T., Verma, V., Bates, J.T., Abrams, J., Klein, M., Strickland, M.J., Sarnat, S.E., Chang, H.H., Mulholland, J.A., Tolbert, P.E., Russell, A.G., Weber, R.J., 2016. Oxidative potential of ambient water-soluble PM2.5 in the southeastern United States: contrasts in sources and health associations between ascorbic acid (AA) and dithiothreitol (DTT) assays. Atmos. Chem. Phys. 16, 3865–3879.
Feng, S., Gao, D., Liao, F., Zhou, F., Wang, X., 2016. The health effects of ambient PM2.5 and potential mechanisms. Ecotoxicol. Environ. Saf. 128, 67–74.
Frezzini, M.A., De Francesco, N., Massimi, L., Canepari, S., 2022. Effects of operating conditions on PM oxidative potential assays. Atmos. Environ. 268, 118802.
Gao, D., Ripley, S., Weichenthal, S., Godri Pollitt, K.J., 2020a. Ambient particulate matter oxidative potential: chemical determinants, associated health effects, and strategies for risk management. Free Radic. Biol. Med. 151, 7–25.
Gao, D., Godri Pollitt, K.J., Mulholland, J.A., Russell, A.G., Weber, R.J., 2020b. Characterization and comparison of PM2.5 oxidative potential assessed by two acellular assays. Atmos. Chem. Phys. 20, 5197–5210.
Ghanem, M., Perdrix, E., Alleman, L.Y., Rousset, D., Coddeville, P., 2021. Phosphate buffer solubility and oxidative potential of single metals or multielement particles of welding fumes. Atmosphere 12, 30.
Giannossa, L.C., Cesari, D., Merico, E., Dinoi, A., Mangone, A., Guascito, M.R., Contini, D., 2022. Inter-annual variability of source contributions to PM10, PM2.5, and oxidative potential in an urban background site in the central Mediterranean. J. Environ. Manage. 319, 115752.
Gonet, T., Maher, B.A., 2019. Airborne, vehicle-derived Fe-bearing nanoparticles in the urban environment: a review. Environ. Sci. Technol. 53 (17), 9970–9991.
Grange, S.K., Uzu, G., Weber, S., Jaffrezo, J., Hueglin, C., 2022. Linking Switzerland's PM10 and PM2.5 oxidative potential (OP) with emission sources. Atmos. Chem. Phys. 22, 7029–7050.
Guo, H., Jin, L., Huang, S., 2020. Effect of PM characterization on PM oxidative potential by acellular assays: a review. Rev. Environ. Health 35 (4), 461–470.
Haynes, E.N., Ryan, P., Chen, A., Brown, D., Roda, S., Kuhnell, P., Wittberg, D., Terrell, M., Reponen, T., 2012. Assessment of personal exposure to manganese in children living near a ferromanganese refinery. Sci. Total Environ. 427–428, 19–25.
Hedayat, F., Stevanovic, S., Miljevic, B., Bottle, S., Ristovski, Z.D., 2015. Review—evaluating the molecular assays for measuring the oxidative potential of particulate matter. Chem. Ind. Chem. Eng. Q. 21, 201–210.
Hernández-Pellón, A., Fernández-Olmo, I., 2019a. Using multi-site data to apportion PM-bound metal(loid)s: impact of a manganese alloy plant in an urban area. Sci. Total Environ. 651 (1), 1476–1488.
Hernández-Pellón, A., Fernández-Olmo, I., 2019b. Airborne concentration and deposition of trace metals and metalloids in an urban area downwind of a manganese alloy plant. Atmos. Pollut. Res. 10 (3), 712–721.
Hernández-Pellón, A., Nischkauer, W., Limbeck, A., Fernández-Olmo, I., 2018. Metal (loid) bioaccessibility and inhalation risk assessment: a comparison between an urban and an industrial area. Environ. Res. 165, 140–149.
Jedynska, A., Hoek, G., Wang, M., Yang, A., Eeftens, M., Cyrys, J., Keuken, M., Ampe, C., Beelen, R., Cesaroni, G., Forastiere, F., Cirach, M., de Hoogh, K., De Nazelle, A., Nystad, W., Akhlaghi, H.M., Declercq, C., Stempfelet, M., Eriksen, K.T., Kooter, I.M., 2017. Spatial variations and development of land use regression models of oxidative potential in ten European study areas. Atmos. Environ. Times 150, 24–32.
Jiang, H., Ahmed, C.M.S., Canchola, A., Chen, J.Y., Lin, Y.H., 2019. Use of dithiothreitol assay to evaluate the oxidative potential of atmospheric aerosols. Atmosphere 10, 571.
Jovanovic, M.V., Savic, J.Z., Salimi, F., Stevanovic, S., Brown, R.A., Jovasevic-Stojanovic, M., Manojlovic, D., Bartonova, A., Bottle, S., Ristovski, Z.D., 2019. Measurements of oxidative potential of particulate matter at Belgrade tunnel; comparison of BPEAnit, DTT and DCFH assays. Int. J. Environ. Res. Public Health 16, 4906.
Kelly, F.J., Fussell, J.C., 2012. Size, source and chemical composition as determinants of toxicity attributable to ambient particulate matter. Atmos. Environ. 60, 504–526.
Khurshid, S.S., Siegel, J.A., Kinney, K.A., 2014. Technical Note: particulate reactive oxygen species concentrations and their association with environmental conditions in an urban, subtropical climate. Atmos. Chem. Phys. 14, 6777–6784.
Ledoux, F., Kfoury, A., Delmaire, G., Roussel, G., El Zein, A., Courcot, D., 2017. Contributions of local and regional anthropogenic sources of metals in PM2.5 at an urban site in northern France. Chemosphere 181, 713–724.
Lelieveld, J., Evans, J.S., Fnais, M., Giannadaki, D., Pozzer, A., 2015. The contribution of outdoor air pollution sources to premature mortality on a global scale. Nature 525, 367–371.
Li, J., Chen, H., Li, X., Wang, M., Zhang, X., Cao, J., Shen, F., Wu, Y., Xu, S., Fan, H., Da, G., Huang, R-jin, Wang, J., Chan, C.K., de Jesus, A.L., Morawska, L., Yao, M., 2019. Differing toxicity of ambient particulate matter (PM) in global cities. Atmos. Environ. 212, 305–315.
Li, R., Yan, C., Meng, Q., Yue, Y., Jiang, W., Yang, L., Zhu, Y., Xue, L., Gao, S., Liu, W., Chen, T., Meng, J., 2024. Key toxic components and sources affecting oxidative potential of atmospheric particulate matter using interpretable machine learning: insights from fog episodes. J. Hazard Mater. 465, 133175.
Ma, Y., Cheng, Y., Qiu, X., Cao, G., Fang, Y., Wang, J., Zhu, T., Yu, J., Hu, D., 2018. Sources and oxidative potential of water soluble humic-like substances .HULISWS/in fine particulate matter (PM2.5) in Beijing. Atmos. Chem. Phys. 18, 5607–5617.
Massimi, L., Ristorini, M., Simonetti, G., Frezzini, M.A., Astolfi, M.L., Canepari, S., 2020. Spatial mapping and size distribution of oxidative potential of particulate matter released by spatially disaggregated sources. Environ. Pollut. 266, 115271.
Massimi, L., Pietrodangelo, A., Frezzini, M.A., Ristorini, M., De Francesco, N., Sargolini, T., Perrino, C., 2022. Effects of COVID-19 lockdown on PM10 composition and sources in the Rome Area (Italy) by elements' chemical fractionation-based source apportionment. Atmos. Res. 266, 105970.
Molina, C., Toro A, R., Manzano, C.A., Canepari, S., Massimi, L., Leiva-Guzmán, M.A., 2020. Airborne aerosols and human health: leapfrogging from mass concentration to oxidative potential. Atmosphere 11 (9), 917.
Moufarrej, L., Courcot, D., Ledoux, F., 2020. Assessment of the PM2.5 oxidative potential in a coastal industrial city in Northern France: relationships with chemical composition, local emissions and long range sources. Sci. Total Environ. 748, 141448.

Ostro, B., Broadwin, R., Green, S., Feng, W.Y., Lipsett, M., 2006. Fine particulate air pollution and mortality in nine California counties: results from CALFINE. Environ. Health Perspect. 114, 29–33.
Otero-Pregigueiro, D., Hernández-Pellón, A., Borge, R., Fernández-Olmo, I., 2018. Estimation of PM10-bound manganese concentration near a ferromanganese alloy plant by atmospheric dispersion modelling. Sci. Total Environ. 627, 534–543.
Pant, P., Harrison, R.M., 2013. Estimation of the contribution of road traffic emissions to particulate matter concentrations from field measurements: a review. Atmos. Environ. 77, 78–97.
Paraskevopoulou, D., Bougiatioti, A., Stavroulas, I., Fang, T., Lianou, M., Liakakou, E., Gerasopoulos, E., Weber, R.J., Nenes, A., Mihalopoulos, N., 2019. Yearlong variability of oxidative potential of particulate matter in an urban Mediterranean environment. Atmos. Environ. 206, 183–196.
Pelfrêne, A., Cave, M.R., Wragg, J., Douay, F., 2017. In vitro investigations of human bioaccessibility from reference materials using simulated lung fluids. Int. J. Environ. Res. Public Health. 14 (2), 112.
Perrone, M.G., Zhou, J., Malandrino, M., Sangiorgi, G., Rizzi, C., Ferrero, L., Dommen, J., Bolzacchini, E., 2016. PM chemical composition and oxidative potential of the soluble fraction of particles at two sites in the urban area of Milan, Northern Italy. Atmos. Environ. 8, 104–113.
Perrone, M.R., Bertoli, I., Romano, S., Russo, M., Rispoli, G., Pietrogrande, M.C., 2019. PM2.5 and PM10 oxidative potential at a Central Mediterranean Site: contrasts between dithiothreitol- and ascorbic acid-measured values in relation with particle size and chemical composition. Atmos. Environ. 210, 143–155.
Pietrogrande, M.C., Russo, M., Zagatti, E., 2019. Review of PM oxidative potential measured with acellular assays in urban and rural sites across Italy. Atmosphere 10, 626.
Pietrogrande, M.C., Bacco, D., Trentini, A., Russo, M., 2021. Effect of filter extraction solvents on the measurement of the oxidative potential of airborne PM2.5. Environ. Sci. Pollut. Res. 28 (23), 29551–29563.
Pietrogrande, M.C., Demaria, G., Colombi, C., Cuccia, E., Dal Santo, U., 2022. Seasonal and spatial variations of PM10 and PM2.5 oxidative potential in five urban and rural sites across Lombardia Region, Italy. Int. J. Environ. Res. Public Health 19 (13), 7778.
Savoie, D.L., Prospero, J.M., 1980. Water-soluble potassium, calcium, and magnesium in the aerosols over the tropical North Atlantic. J. Geophys. Res. 85, 385–392.
Shahpoury, P., Zhang, Z.W., Filippi, A., Hildmann, S., Lelieveld, S., Mashtakov, B., Patel, B.R., Traub, A., Umbrio, D., Wietzoreck, M., Wilson, J., Berkemeier, T., Celo, V., Dabek-Zlotorzynska, E., Evans, G., Harner, T., Kerman, K., Lammel, G., Noroozifar, M., et al., 2022. Inter-comparison of oxidative potential metrics for airborne particles identifies differences between acellular chemical assays. Atmos. Pollut. Res. 13 (12), 101596.
Simonetti, G., Conte, E., Perrino, C., Canepari, S., 2018. Oxidative potential of size-segregated PM in an urban and an industrial area of Italy. Atmos. Environ. 187, 292–300.
Szigeti, T., Óvári, M., Dunster, C., Kelly, F.J., Lucarelli, F., Záray, G., 2015. Changes in chemical composition and oxidative potential of urban PM2.5 between 2010 and 2013 in Hungary. Sci. Total Environ. 518–519, 534–544.
Taghvaee, S., Sowlat, M.H., Diapouli, E., et al., 2019. Source apportionment of the oxidative potential of fine ambient particulate matter (PM2.5) in Athens, Greece. Sci. Total Environ. 653, 1407–1416.
Veld, M., Pandolfi, M., Amato, F., et al., 2023. Discovering oxidative potential (OP) drivers of atmospheric PM10, PM2.5, and PM1 simultaneously in North-Eastern Spain. Sci. Total Environ. 857 (2), 159386.
Verma, V., Fang, T., Guo, H., King, L., Bates, J.T., Peltier, R.E., Edgerton, E., Russell, A. G., Weber, R.J., 2014. Reactive oxygen species associated with water-soluble PM2.5 in the southeastern United States: spatiotemporal trends and source apportionment. Atmos. Chem. Phys. 14, 12915–12930.
Verma, V., Wang, Y., El-Afifi, R., Fang, T., Rowland, J., Russell, A.G., Weber, R.J., 2015. Fractionating ambient humic-like substances (HULIS) for their reactive oxygen species activity – assessing the importance of quinones and atmospheric aging. Atmos. Environ. 120, 351–359.
Weber, S., Uzu, G., Calas, A., Chevrier, F., Besombes, J.L., Charron, A., Salameh, D., Ježek, I., Močnik, G., Jaffrezo, J.L., 2018. An apportionment method for the oxidative potential of atmospheric particulate matter sources: application to a one-year study in Chamonix, France. Atmos. Chem. Phys. 18, 9617–9629.
Weber, S., Uzu, G., Favez, O., Borlaza, L.J.S., Calas, A., Salameh, D., Chevrier, F., Allard, J., Besombes, J.L., Albinet, A., Pontet, S., Mesbah, B., Gille, G., Zhang, S., Pallares, C., Leoz-Garziandia, E., Jaffrezo, J.L., 2021. Source apportionment of atmospheric PM10 oxidative potential: synthesis of 15 year-round urban datasets in France. Atmos. Chem. Phys. 21, 11353–11378.
White, W.H., 2008. Chemical markers for sea salt in IMPROVE aerosol data. Atmos. Environ. 42 (2), 261–274.
WHO, 2021. WHO Global Air Quality Guidelines 2021. World Health Organization.
Yu, Y., Cao, J., 2023. Chemical fingerprints and source profiles of PM10 and PM2.5 from agricultural soil in a typical polluted region of northwest China. Aerosol Air Qual. Res. 23 (6), 220419.